Wind-Flow Patterns in the Grand Canyon as Revealed by Doppler Lidar

ROBERT M. BANTA AND LISA S. DARBY

Environmental Technology Laboratory, NOAA/Environmental Research Laboratory, Boulder, Colorado

PIRMIN KAUFMANN, DAVID H. LEVINSON, AND CUI-JUAN ZHU

Cooperative Institute for Research in Atmospheric Sciences, University of Colorado, and NOAA/Environmental Technology Laboratory, Boulder, Colorado

(Manuscript received 15 December 1997, in final form 22 July 1998)

ABSTRACT

Many interesting flow patterns were found in the Grand Canyon by a scanning Doppler lidar deployed to the south rim during the 1990 Wintertime Visibility Study. Three are analyzed in this study: 1) flow reversal in the canyon, where the flow in the canyon was in the opposite direction from the flow above the canyon rim; 2) under strong, gusty flow from the southwest, the flow inside and above the canyon was from a similar direction and coupled; and 3) under light large-scale ambient flow, the lidar found evidence of local, thermally forced up- and down-canyon winds in the bottom of the canyon.

On the days with flow reversal in the canyon, the strongest in-canyon flow response was found for days with northwesterly flow and a strong inversion at the canyon rim. The aerosol backscatter profiles were well mixed within the canyon but poorly mixed across the rim because of the inversion. The gusty southwest flow days showed strong evidence of vertical mixing across the rim both in the momentum and in the aerosol backscatter profiles, as one would expect in turbulent flow. The days with light ambient flow showed poor vertical mixing even inside the canyon, where the jet of down-canyon flow in the bottom of the canyon at night was often either cleaner or dirtier than the air in the upper portions of the canyon. In a case study presented, the light ambient flow regime ended with an intrusion of polluted, gusty, southwesterly flow. The polluted, high-backscatter air took several hours to mix into the upper parts of the canyon. An example is also given of high-backscatter air in the upper portions of the canyon being mixed rapidly down into a jet of cleaner air in the bottom of the canyon in just a few minutes.

1. Introduction

To visitors at Grand Canyon National Park (GCNP) the most important altitude levels for visibility are at and below the canyon rim. Here the visibility is most affected by aerosol concentrations in the atmosphere between the viewer's vantage point on one side of the canyon and the geological formations within and on the other side of the canyon. One of the charms of these spectacular vistas is that differences in the angle and intensity of the sun's lighting through the day cause the appearance of these formations to change dramatically in character and coloration, provided they are visible and sufficiently illuminated. Atmospheric haze dulls the colors.

Haze-producing aerosols are often advected into the canyon area from sources or source regions, sometimes local and sometimes hundreds of kilometers distant. Thus, a key issue for within-canyon visibility is the effectiveness of the vertical transport of haze pollutants down into and within the canyon. And, because cleaner air can also be advected in from elsewhere, it is of interest to determine how efficiently the canyon can be cleaned out. To understand these vertical transports it is critical to understand the relationship between the flow structure within the canyon, which redistributes aerosols there, and external parameters, such as the direction and speed of the synoptic winds above the canyon rim and the static stability between the air in the canyon and the air just above, including the presence and strength of inversions or stable layers at or below rim level.

In the present study we use measurements from the 1990 Wintertime Visibility Study (WVS) to investigate 1) the relationship between flow structure in the canyon and external conditions and 2) mixing between the air in the canyon and the air just above. The purpose of the WVS and a description of the instrumentation deployed for the WVS is described by Lindsey et al. (1999). The primary instrument for the present study is

Corresponding author address: Dr. Robert M. Banta, NOAA/ERL (ET2), 325 Broadway, Boulder, CO 80303.
E-mail: rbanta@etl.noaa.gov

the Doppler lidar, which was sited on the south rim of the canyon at Navajo Point by the Environmental Technology Laboratory (ETL) of the National Oceanic and Atmospheric Administration's Environmental Research Laboratories (NOAA/ERL). We use winds above the rim top measured by the Doppler lidar and radiosonde. The static stability was determined by radiosonde, tethersonde, and pairings of surface mesonet stations on the canyon rim with stations within the canyon. The structure of the flow and aerosol profiles inside the canyon were probed using lidar-scan data. In this paper ''the rim,'' ''rim top,'' or ''rim level'' without further qualification will refer to the south rim at the location of the lidar at an elevation of 2285 m.

For the January–March 1990 study period, the Doppler lidar revealed many different flow structures in the canyon, but three frequent patterns were noted.

1) Reversed flow: flow in the canyon was opposite to the direction of the large-scale flow just above the rim. This flow occurred most often under northwesterly synoptic winds.
2) Coupled southwesterly flow: flow in the canyon was in the same direction as the flow above and very turbulent, generally occurring under southwesterly synoptic flow.
3) Thermally forced along-canyon flow: during the light-wind period in early March 1990, local, thermally forced, up- and down-canyon flows occurred.

In the following study we investigate the typical flow structure and vertical mixing characteristics of each of these flow patterns.

2. Background

The dependence of flow within a depression, valley, or canyon on external parameters such as cross-valley wind flow and stability has received some attention in the literature. Scorer (1978) observed that a large-scale wind blowing transverse to a large valley or canyon may produce a variety of responses in the valley, including a reverse-flow eddy that occupies the entire valley. Tang (1976) found steady-state solutions to flow in a valley for unstable daytime and stable nighttime conditions with cross flow aloft. Both solutions produced reverse-flow eddies in the valley, the daytime cell favoring the upwind slope and the nighttime favoring the downwind slope. Bell and Thompson (1980) related flows in the valley to a Froude number using the external flow speed and the static stability across the top of the valley. Cunningham and Bedard (1993) performed laboratory studies of the dissolution and removal of a stable layer in a valley by ambient flow aloft, including interesting flow visualization of the stages they found. A more recent area of active interest is urban street canyons, where the flows can flush or trap air pollutants. A variety of circulations have been noted, depending on the external flow and the stability (Oke 1988; Rotach 1993a,b; Sini et al. 1996).

In the Grand Canyon, Stearns (1987) found evidence of reversed flow in measurements from a surface station in the canyon during periods when the above-canyon winds had a significant cross-canyon component. Gaynor and Banta (1991) studied flow in the Grand Canyon during the 1990 WVS on two days that appeared to have cross-canyon flow, one of which had a strong inversion near the rim top and the other of which had no evidence of an inversion at that level.

a. Wintertime visibility study

The WVS was sponsored by the Salt River Project of Phoenix, Arizona. It took place in the Grand Canyon region of northern Arizona and southern Utah in 1990 to investigate possible effects that emissions from the Navajo Generating Station (NGS) power plant might have on visibility in the Grand Canyon (Chan and Bhardwaja 1991; Lindsey et al. 1999; Whiteman et al. 1999b; Richards et al. 1991). The project included perfluorocarbon tracer releases from the NGS. During the WVS the Doppler lidar was situated at the eastern end of the south rim of the Grand Canyon at the Navajo Point viewpoint, as shown in Fig. 1. Several other instrument sites important to the study are also identified in Fig. 1. A detailed description of the surface-instrumentation sites and meteorological characteristics of each site during the WVS is given by Hauser et al. (1991), and the effects of local topography at each site on the diurnal wind patterns are described by Whiteman et al. (1999a).

The local, thermally forced wind systems that form in the Grand Canyon region of the western United States on synoptically quiet days are complicated by the highly complex nature of the topography, as demonstrated by Whiteman et al. (1999a). Two effects are important to this study. First, the topography in the Grand Canyon dramatically drops to a shelf 1000–1500 m below the high ground at the north and south rims, but then into this relative ''bottom'' the Colorado River has cut a sharp notch that is another 500–800 m deep. In this study we shall refer to this lowest part of the canyon as the Colorado River ''gorge.'' The flow in this gorge can be different from the flow higher in the canyon.

Second, as the Colorado River flows through the area from Page, Arizona, north-northeast of the region depicted in Fig. 1, to the Grand Canyon north of Desert View, it cuts through a plain that slopes downward from the Kaibab Plateau toward the Page/Lake Powell area to the northeast (NE). This sloping plain, referred to as the Marble Platform, thus slopes downward to the NE, the opposite direction to the slope of the Colorado River gorge (Whiteman et al. 1999a; Lindsey et al. 1999), since the river flows from NE to SW (southwest). A downslope flow along the platform will thus appear to be an upvalley flow with respect to the Colorado River

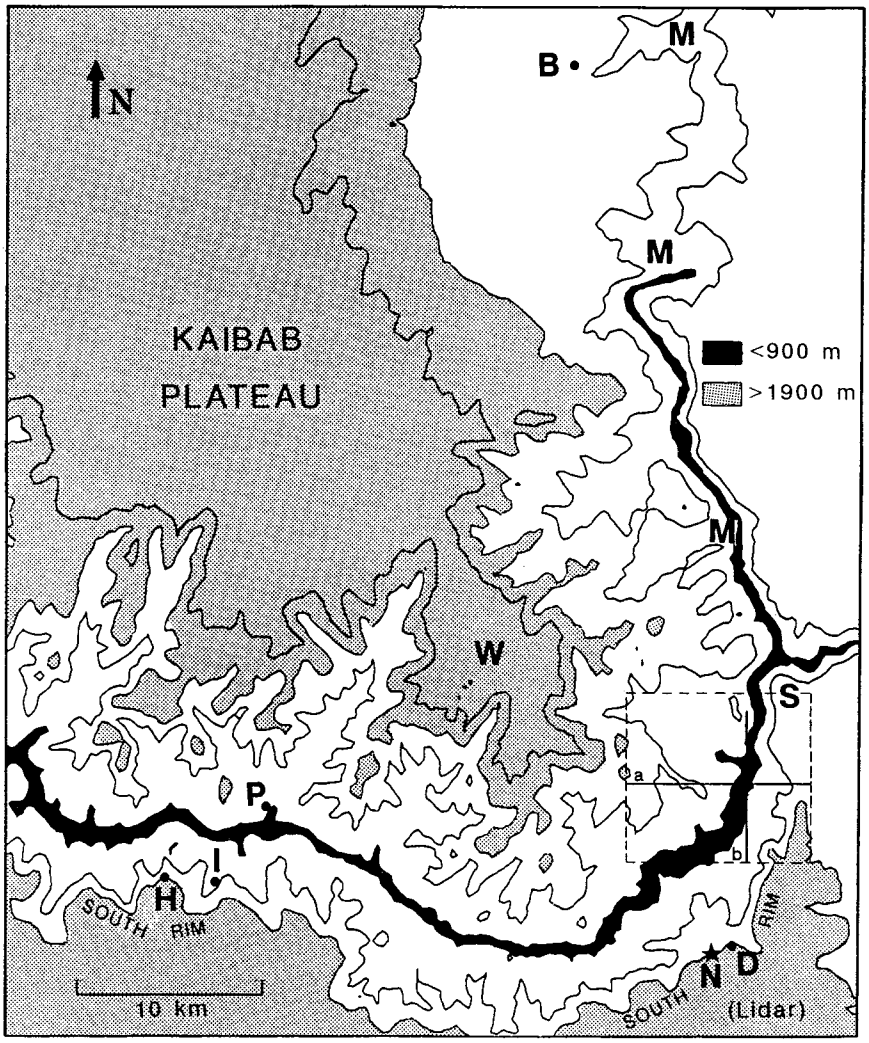

FIG. 1. Map of Grand Canyon and vicinity. The Doppler lidar was situated at Navajo Point (N), 1 km west of Desert View (D). Contours are at 500-m intervals, from 900 to 2400 m MSL, and terrain between 900 and 1900 m is shown as white. The dashed box represents the area plotted in Fig. 10a, and the solid lines marked a and b show the locations of cross- and along-canyon cross sections in Figs. 10b–c. The following other locations are shown: B, Buffalo Ranch; H, Hopi Point; I, Indian Garden; M, Marble Canyon; P, Phantom Ranch; S, Cape Solitude; and W, Walhalla Plateau.

flow direction. Because the slope flows dominate on the platform at sites such as Buffalo Ranch, the diurnal behavior of the flows is at apparent odds with the traditional thermally forced along-valley wind model, if this region were considered to be the valley of the Colorado River (Whiteman et al. 1999a,b).

b. ETL's Doppler lidar

ETL's pulsed Doppler lidar transmits a beam of coherent, eye-safe infrared (IR) (wavelength 10.59 μm) radiation into the atmosphere. The pulse is scattered by aerosol particles, and a small amount of the energy is returned (backscattered) to the lidar. The intensity and frequency of this backscattered energy represents the spatial distribution of aerosol particles and their speed of movement along the lidar beam, respectively. Because the aerosols detected by the lidar are small enough to be excellent tracers of air motion, the Doppler shift in the frequency of the returned IR signal can be used to calculate the component of the wind along the lidar beam, or radial wind velocity u_r. Range gates for this lidar are at 300-m intervals, and the velocity accuracy is 60 cm s^{-1} (Post and Cupp 1990). Other characteristics of the lidar during the WVS are shown in Table 1.

ETL's Doppler lidar, described by Post and Cupp (1990), has been used to provide wind and aerosol backscatter information to study a wide variety of mesoscale

TABLE 1. Characteristics of the Doppler lidar during the WVS.

Lidar specifications	
Wavelength (μm)	10.59
Maximum range (km)	up to 30.00
Minimum range (km)	1.20
Range resolution (km)	0.30
Beam width (μrad) [°]	90.00 [0.005]
Rms velocity accuracy (cm s^{-1})	60.00
Pulse repetition frequency (Hz)	10.00
Pulses averaged	3.00
Effective pulse rate (Hz)	3.33
Standard scan rate (°s^{-1})	3.33
Angular resolution (°)	1.00

atmospheric flow systems. For example, wind and aerosol information from the lidar were used together to study a prescribed forest fire (Banta et al. 1992) and the transport of polluted air into and out of a tributary of the Fraser River Valley by the diurnal wind systems near Vancouver, British Columbia, Canada (Banta et al. 1997; McKendry et al. 1998). The lidar was also used to study a number of other small mesoscale flows, including complex-terrain flows (Post and Neff 1986; Neff 1990; Levinson and Banta 1995; Banta et al. 1995, 1996) and the sea breeze (Banta 1995).

Post (1978) and Banta et al. (1992) found that, for typical size distributions of atmospheric aerosols, the maximum contribution to backscatter from a CO_2 lidar comes from particles of about 1 μm radius. These particles are much larger than those that affect visible light and restrict visibility. On many occasions we observed reductions in visibility at the Grand Canyon before observing an increase in lidar backscatter, and conversely we also observed improving visibility at times when lidar aerosol backscatter remained high. This illustrates that the relationship between lidar backscatter and visibility or transmissometer readings is a complicated function of aerosol concentration, composition, size distribution, and other characteristics, although they are frequently correlated.

During the WVS, we used azimuth and elevation scans [plan-position indicator (PPI) and range-height indicator (RHI) scans in radar terms, respectively] to investigate the atmosphere above the canyon rim. Within and just below the rim, where we wanted fine resolution, we also performed stepped horizontal or vertical scans to obtain data in three-dimensional (3D) volumes.

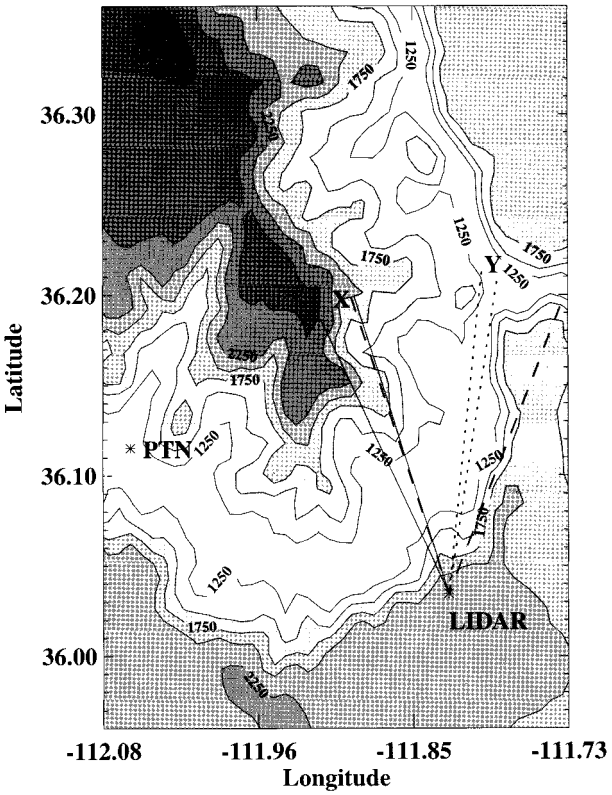

FIG. 2. Map showing the azimuth range of the two-stepped azimuth, vertical-slice scans, and the stepped-elevation (HR) scan sequence described in Table 1. The X indicates the cross-canyon vertical-slice sequence (VRXS), and Y the along-canyon sequence (VRGC). Dashed lines show the limits of the azimuth scans for HR. Also shown are the locations of the lidar and Phantom Ranch (PTN). Terrain contours are at 250-m increments, and terrain less than 1250 m MSL is shown as white.

These volume scans were analyzed using software developed for Doppler radar data, by first transforming the data from spherical coordinates into Cartesian coordinates (Mohr et al. 1986).

We employed a variety of scanning strategies during the WVS, depending on flow conditions, but in this paper we focus on three types as listed in Table 2: vertical slices across the canyon to the northwest (X in Fig. 2), vertical slices along the canyon to the north toward Marble Canyon (Y in Fig. 2), and 3D volume scans. We analyzed data from four such volume scans. All

TABLE 2. Scans analyzed for this paper. Designations X and Y are illustrated in Fig. 2. The θ is the azimuth angle from north, and ϕ, the elevation angle from horizontal. The $\Delta\theta$ and $\Delta\phi$ refer either to the step increment or to the scanning rate (when preceded by "@").

Name	Type	θ_{min}	θ_{max}	$\Delta\theta$	ϕ_{min}	ϕ_{max}	$\Delta\phi$	Designation
VRXS	Stepped RHI	327.7°	336.7°	1.0°	−14.3°	30.0°	@1.67° s^{-1}	Cross-canyon vertical slice, X
VRGC	Stepped RHI	8.0°	12.5°	0.5°	−12.0°	30.0°	@1.67° s^{-1}	Along-canyon vertical slice, Y
HR	Stepped PPI	336.0°	28.0°	@1.33° s^{-1}	−12.0°	2.0°	0.5°	Along-canyon volume scan: Full
HRMED	Stepped PPI	350.0°	15.0°	@1.67° s^{-1}	−12.0°	0.0°	0.5°	" Medium resolution
HRHI2	Stepped PPI	2.0°	15.0°	@1.00° s^{-1}	−12.5°	−0.5°	0.25°	" High resolution
HRHIHI	Stepped PPI	8.0°	12.6°	@1.00° s^{-1}	−9.0°	−3.0°	0.25°	" High resolution, small volume

volume scans were performed at a slower scanning rate than the standard rate listed in Table 1 to achieve finer transverse spatial resolution. One volume scan (HR) consisted of 29 nearly horizontal sector scans (i.e., azimuth scans) taken from 336° to 28° in azimuth and every 0.5° in elevation from 12° below the canyon rim to 2° above the rim. This scan covered the opening of the canyon to the north, from the eastern sidewall to the Walhalla Plateau on the west (between the dashed lines on Fig. 2), but it took 20 min to complete. The other scans took less time. HRMED used a slightly faster scanning rate and relaxed the resolution over a smaller volume. The other two scans (HRHI2 and HRHIHI) were at finer transverse resolution, but over a much more focused volume. Three-dimensional volumes consisting of stepped vertical scans were also taken during the WVS, but the volume covered was offset from the area of interest here, so they were not used in this study.

When the lidar scanned to the north, the measured u_r closely matched the along-canyon flow in the Grand Canyon. For reference, 0.5° data intervals provided resolutions of <90 m at 10-km range, and a 1.67° s^{-1} scanning rate gave data at 0.5° intervals in the sweep direction, at that distance and at the 3⅓ Hz effective beam repetition frequency employed.

Other important scans were full 360° azimuth scans at various elevation angles. We analyzed these scans using the velocity-azimuth display technique (Browning and Wexler 1968) to obtain profiles of the horizontal wind. Profiles from scans at 15° elevation were used to determine the ''ambient winds'' referred to in the text, using the lowest few range gates, which were at a height of 300–400 m above the level of the lidar.

c. Measurements of stability

An important quantity in interpreting the relationship between the flow inside and outside of the canyon is the stability or temperature difference between the atmosphere within and just above the canyon. Sutherland (1991) found that during the WVS, days with higher stabilities ($\partial T/\partial z > 5$ C km^{-1}) had better visibility than lower stability days (which predominantly occurred under southwesterly flow).

We determined the stability in two ways. First, we used the temperature-sounding data from the airsonde, the type of radiosonde used in this study, launched from Phantom Ranch [750 m above mean sea level (MSL)], for levels within and above the rim of the canyon. Figure 3d shows the distribution of stabilities determined in this manner for the entire six weeks of the WVS. Second, we used two surface stations, either Desert View or Hopi Point, which were perched on the south rim of the canyon (2283 m and 2152 m MSL, respectively), paired with Indian Garden, which is located in the canyon (1146 m MSL; see Fig. 1). The stability was calculated by dividing the measured temperature difference between stations by their elevation difference. This approach is similar to that employed by Sutherland (1991).

Such stability determinations were made for all available hours of the WVS for the Hopi Point–Indian Garden and Desert View–Indian Garden surface-station pairings (Figs. 3a,b). The distributions are similar in that a large percentage of the values was near neutral (i.e., rather unstable), in agreement with the findings of Whiteman et al. (1999b). Figure 3c shows only those surface-station-pair values that occurred at times when airsonde data were also available. This histogram indicates a bias toward more stable values in this smaller sample (Fig. 3c) than in the ''all-hours'' distribution (Fig. 3a). This bias is most likely related to the fact that intensive-measurement periods (with more frequent soundings) were called when conditions favored transport from NGS to GCNP, which would tend to be periods of greater stability than normal. The stability distribution directly from the soundings (Fig. 3d) also shows a greater frequency of stable conditions than the all-hours distributions.

The advantage of using rawinsonde information is that inversion strengths and heights can be accurately determined; however, the sample size is relatively small. The advantage of using surface stations is a much larger sample size and a better chance of getting data at the time when other (e.g., lidar) data are available. Drawbacks are that each station is susceptible to local and other surface effects, which are a function of ambient stability and wind direction, and this method does not show when an inversion occurs above the rim, as occasionally happens (Whiteman et al. 1999b). Because of the desirability of using the more frequent station-pair estimates, we directly compared the stability determined in this way with the airsonde stability estimates for the same layer, using the station-pair values at the nearest hour. The results show general agreement whether Indian Garden is paired with Hopi Point or Desert View (Fig. 4). Thus, in spite of the difficulties mentioned, the differences between stability measured by airsonde and by station pairs, as indicated by Fig. 4 and the distributions in Figs. 3c,d, are relatively small. This agrees with Sutherland's (1991) findings based on morning (~0800 MST) soundings with data from the Hopi Point–Indian Garden site pairings.

3. Results

The three patterns of flow in the Grand Canyon identified in section 1 are illustrated in Fig. 5. The flow reversal at the canyon rim is evident in Fig. 5a, as is the turbulent structure of the southwesterly flow in Fig. 5b. The cross-canyon cross section in Fig. 5c shows the jet of northerly down-canyon flow in the bottom of the canyon at a range of 9.9 km from the lidar site at Navajo Point. Such vertical cross sections are available every 300 m from the minimum range of the lidar to the farthest range the lidar can see.

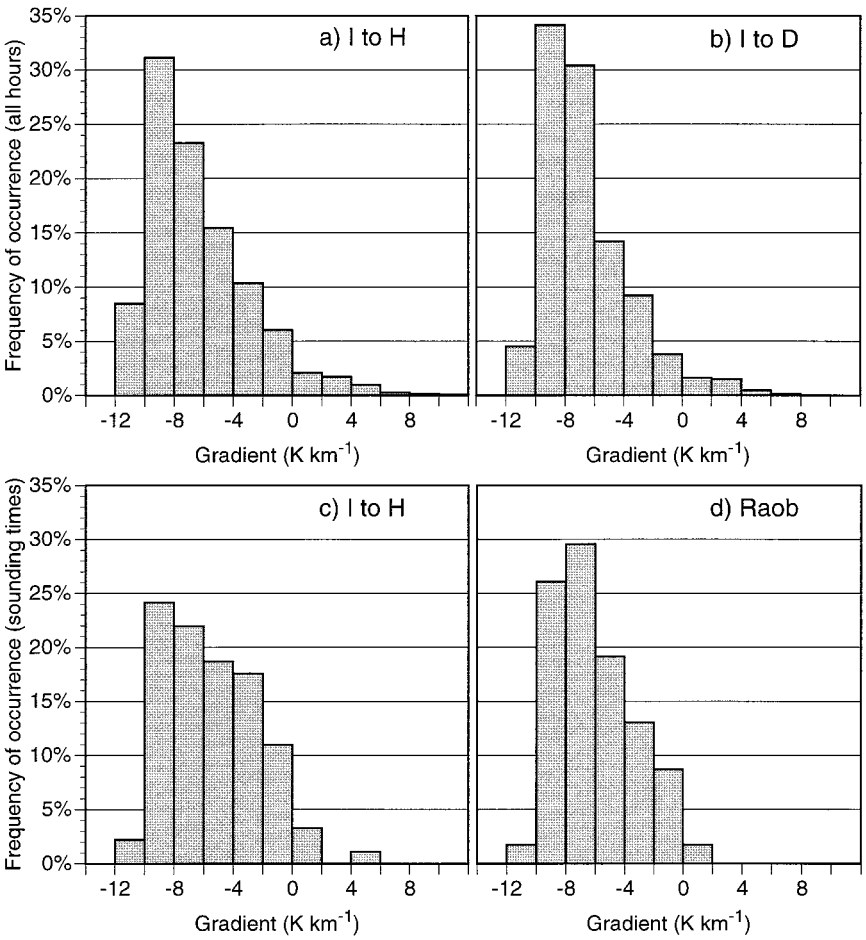

FIG. 3. Histograms of the frequency of occurrence of temperature gradients. Upper panels: gradient for all hours from 10 January to 19 March 1990: (a) between Indian Garden and Hopi Point; (b) between Indian Garden and Desert View. Lower panels: (c) mean temperature gradient between Indian Garden and Hopi Point at only those hours with sounding data available; (d) mean gradient between the 400- and 1400-m sounding levels, corresponding to the heights above Phantom Ranch of Indian Garden (1146 m) and Hopi Point (2152 m).

a. Reversed flow

From the vantage point of the lidar on the south rim and the orientation of the cross-canyon scans (indicated by X on Fig. 2), the best wind directions for studying cross-canyon flow would be northwesterly (NW) or southeasterly (SE). Several cases of NW flow occurred while the lidar was operating during the WVS, but no cases of extended SE winds occurred. The few cases of easterly flow occurred mostly with light winds at the canyon rim. Gaynor and Banta (1991) studied the flow on two NW ambient-wind days, one with a strong inversion just below the level of the south rim, and one with much weaker stability across the canyon rim, but with indications of a weak inversion above the level of the north rim (~1700 m above Phantom Ranch, or 2450 m MSL). They found reversed flow in the canyon in both cases, using lidar cross sections on 23 January (inversion present) and the UHF wind profiler at Phantom Ranch on 24 January (inversion absent). Because of the distance from Phantom Ranch to the lidar and the potential for ground-clutter contamination in the profiler winds below the rim (see Whiteman et al. 1999b), we analyzed canyon cross-sectional scans on 24 January to see whether the lidar also detected the flow reversal from its location.

1) IN-CANYON FLOW

An extended period of NW ambient flow of ~5 m s^{-1} on 20–21 February produced a strong reversal of flow in the canyon. Velocity profiles taken in the middle of the canyon show that this reversed flow reached nearly 4 m s^{-1} (Fig. 6). The strong inversion in the potential-temperature θ sounding at about the level of the south rim and the reversal of flow in the canyon bear a strong resemblance to Gaynor and Banta's 23 January case.

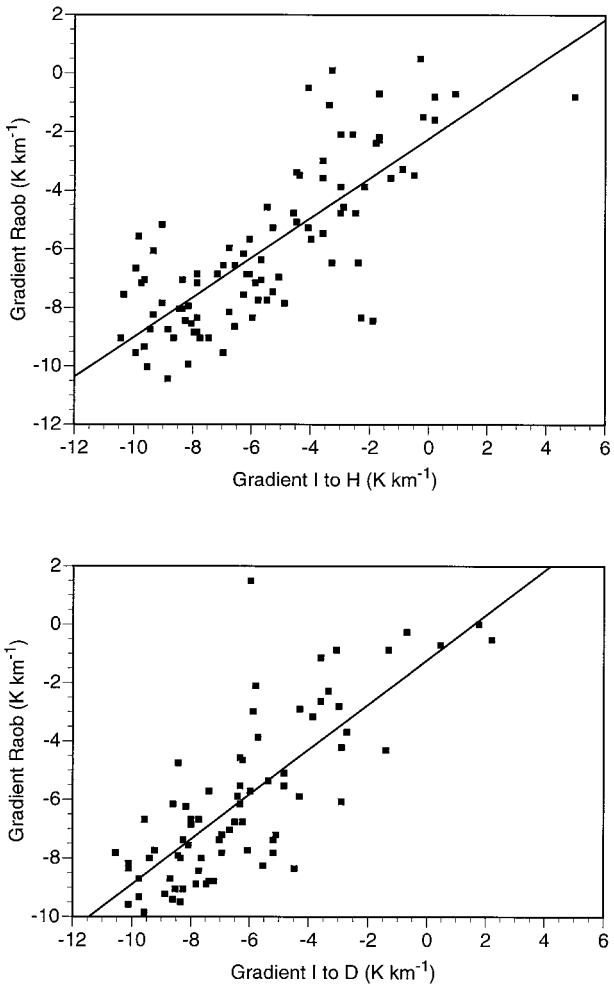

FIG. 4. Scatter diagrams of temperature gradients calculated from surface stations (x axis) and from soundings at the corresponding heights (y axis). Top panel: gradients between heights of Indian Garden and Hopi Point (correlation coefficient $r = 0.78$). Bottom panel: gradients between heights of Indian Garden and Desert View ($r = 0.78$).

The θ profiles from both study periods were included in Whiteman et al.'s (1999b) sample of Phantom Ranch soundings showing θ jumps at near-rim elevations (see their Fig. 11).

For contrast, profiles for 24 January, the day without a strong stable layer at the rim, are shown in Fig. 7. The u_r profile shows a sharp reduction of flow in the canyon, but the flow was in the same direction as the ambient flow aloft, that is, no reversal. This profile was taken near midday (1800 UTC is 1100 MST) on 24 January.

A time plot of hourly values of the station-pair stability estimates for the two days of NW flow (23–24 January) is given in Fig. 8. It shows strong stability, as noted by Gaynor and Banta (1991), on 23 January, when lidar data indicated strong flow reversal in the canyon very similar to that in Figs. 5a and 6. The stability steadily weakened until, for several hours around midday on 24 January, it was nearly neutral. The symbols indicate that the airsonde stabilities agreed closely with the trend in the station-pair stabilities for this period. Between 0800 and 1700 UTC on 24 January, the stability was intermediate between the strong stability on the day before and weak stability later on 24 January. During this period lidar u_r cross sections indicated a weak and disorganized flow reversal in the canyon of less than 2 m s^{-1} (not shown). Thus, using lidar data from Navajo Point, we found weak reversal early in the day and no reversal at midday on 24 January (Fig. 7). We did not find clear evidence of the reversal of flow in the canyon that Gaynor and Banta (1991) found at Phantom Ranch using profiler data.

Thus, rim-top stability seemed to be a strong control on the degree of flow reversal in the canyon, for sufficiently strong ambient cross-canyon flow. Cases with cross-canyon ambient flow $\gtrsim$5 m s^{-1} and a strong inversion at the rim generated a distinct flow reversal in the canyon, but the flow reversal was not produced when the rim-top stability was near neutral. Intermediate stabilities produced an intermediate flow condition, namely, a weak, disorganized reversal of flow.

2) VERTICAL MIXING

Aerosol backscatter profiles on 20–21 February indicated a sharp difference across the rim-top inversion, but a relatively well-mixed profile within the canyon below the inversion (Fig. 6). The profile on the day with lower stability at the rim top (Fig. 7) shows a weaker gradient over a greater depth at the rim, indicating stronger mixing across this level than in the strong-inversion case, in agreement with the conclusions based on the θ profiles.

b. Coupled southwesterly flow

Days with warm SW flow, typically $\gtrsim$10 m s^{-1}, occurred several times during the WVS. On occasion the flow was widespread and persistent enough that pollution and haze from the southern California urban basins could be tracked across southern California, southern Nevada, northern Arizona, and into the Grand Canyon area. Flow regimes from a southerly direction, including this SW one, are responsible for summertime haze in the Grand Canyon but are less common during the cold season. Nevertheless, Lindsey et al. (1999) show that most periods of significant visibility reduction in GCNP during the WVS occurred under these conditions.

1) IN-CANYON FLOW

Vertical-slice scans taken along the canyon to the north (indicated by Y in Fig. 2) show that on days with SW ambient winds the flow in the canyon was in the

same direction as the winds above. The strong variability and turbulent structure of the winds indicate eddies extending across the level of the canyon rim (Fig. 5b). The eddies had a horizontal scale of 3–5 km, tending to increase somewhat in time. The u_r profile for 7–8 February 1990, a typical day with SW flow, indicates a profile increasing with height from inside to above the canyon (Fig. 9) and exhibiting turbulent variability. This is consistent with the absence of an inversion in the θ profile near rim level.

2) VERTICAL MIXING

The aerosol backscatter profile for 7–8 February (Fig. 9) is nearly constant with height from the bottom of the canyon to ~700 m above the south rim. This is also consistent with the highly turbulent environment and absence of stable layers. The nearly constant profile is maintained in spite of a clean, low-backscatter layer above 1 km above lidar level (ALL), which had probably advected into the area from elsewhere.

c. Thermally forced along-canyon flow

During most of the WVS the winds were relatively strong (>5 m s^{-1}), and light-wind periods were mostly short and transitional. However, an extended period of weak synoptic flow began at the end of February and extended into the first days of March.

Whiteman et al. (1999b) showed that, under stronger large-scale flow and pressure gradients, the winds in the upper portions of the canyon at Phantom Ranch were produced by channeling of the flow aloft or channeling induced by the horizontal, along-canyon pressure difference. An important remaining question is, what happens to the winds in the canyon when the large-scale forcing is weak? Such periods often produce thermally forced along-valley flows in mountain valleys and might be expected to generate diurnal flows along the canyon axis. These flows would be down canyon at night and up canyon during the day, where down canyon would generally be from a northerly or easterly direction (i.e., the same direction as the flow of the Colorado River), and up canyon would be the opposite, as described in section 2a. Whiteman et al. (1999b), however, concluded from tethersonde wind data at Phantom Ranch that such diurnal flows do not occur there, and, in fact, surface-station data show that the flow, though weak, tends to be up canyon at night and down canyon during the day there, contrary to expectations (Whiteman et al. 1999a). In the following section we use 3D volume scans during the light-wind period from 28 February to 2 March to investigate whether diurnal flows occurred in the north–south region of the Grand Canyon to the north of Desert View.

We address this question here, but also include data for 3–5 March, the three days following the light-wind period. On 3 March snow fell at GCNP, and at night on 3 March into the morning of 4 March the ambient winds again became light. On the afternoon of 4 March a transition to strong southwesterly synoptic winds began. The SW flow increased in speed until just before a second snowfall commenced starting at ~1500 UTC on 5 March.

1) IN-CANYON FLOW

Under light ambient-wind conditions, the flow in the canyon was best revealed by along-canyon volume scans as indicated in Table 2. Analyses of the full volume scan for 0900 UTC (0200 MST) on 28 February are shown in Figs. 10–11. The major organized feature was a jet of northerly wind near the bottom of the canyon flowing down from Marble Canyon toward the lidar site. Figure 10 shows three orthogonal slices through this jet. The core of down-valley flow is represented by the dash-contoured, 3–4 m s^{-1} channel (shaded), embedded in a region of lighter wind speeds of generally less than 2 m s^{-1}. The horizontal slice (Fig. 10a) shows the continuity of the jet as it flowed southward along the Colorado River gorge at a depth of 1.2 km below the level of the lidar (i.e., at $z = -1.2$ km). The jet, flowing from north to south, bent to the west as it flowed southward past $y = 7$ km and was channeled by the curving terrain of the lower canyon. Figure 10b is an along-canyon vertical slice showing the vertical structure of the down-canyon jet and the flow reversal ~700 m below the rim. The cross-canyon slice (Fig. 10c) shows the same perspective as Fig. 5c, which was from a different day (2 March), but also at night (1256 UTC, or 0556 MST). Both show similar features of the flow, including the down-canyon jet.

February 28 was interesting because it was identified by Lindsey et al. (1999) as a day when NGS emissions appeared at GCNP. Unlike nearly all the other such days, however, it did not have persistent synoptic north-north-

→

FIG. 5. Doppler lidar radial velocity measurements. Green and blue represent flow toward the lidar, whereas yellow and red represent flow away. Tick marks are at 2-km (horizontal) and 1-km (vertical) increments. The lidar was located at (0, 0); thus $z = 0$ represents the height of the south rim. (a) A cross-canyon scan (azimuth = 331.8°) taken on 21 February 1990, demonstrating a flow reversal at rim height (the flow above the rim had a northwesterly component and the flow below the rim had a southeasterly component). (b) An along-canyon scan (azimuth = 10°) taken on 7 February 1990, showing strong, gusty winds above and in the canyon. The missing data areas between the red and pink regions are due to weak backscatter returns, i.e, relatively cleaner air. (c) A vertical slice of a volume scan looking north, taken from range gates a constant distance of 9.9 km from the lidar. The blue and green regions represent northerly along-canyon flow, and the warmer colors represent southerly flow.

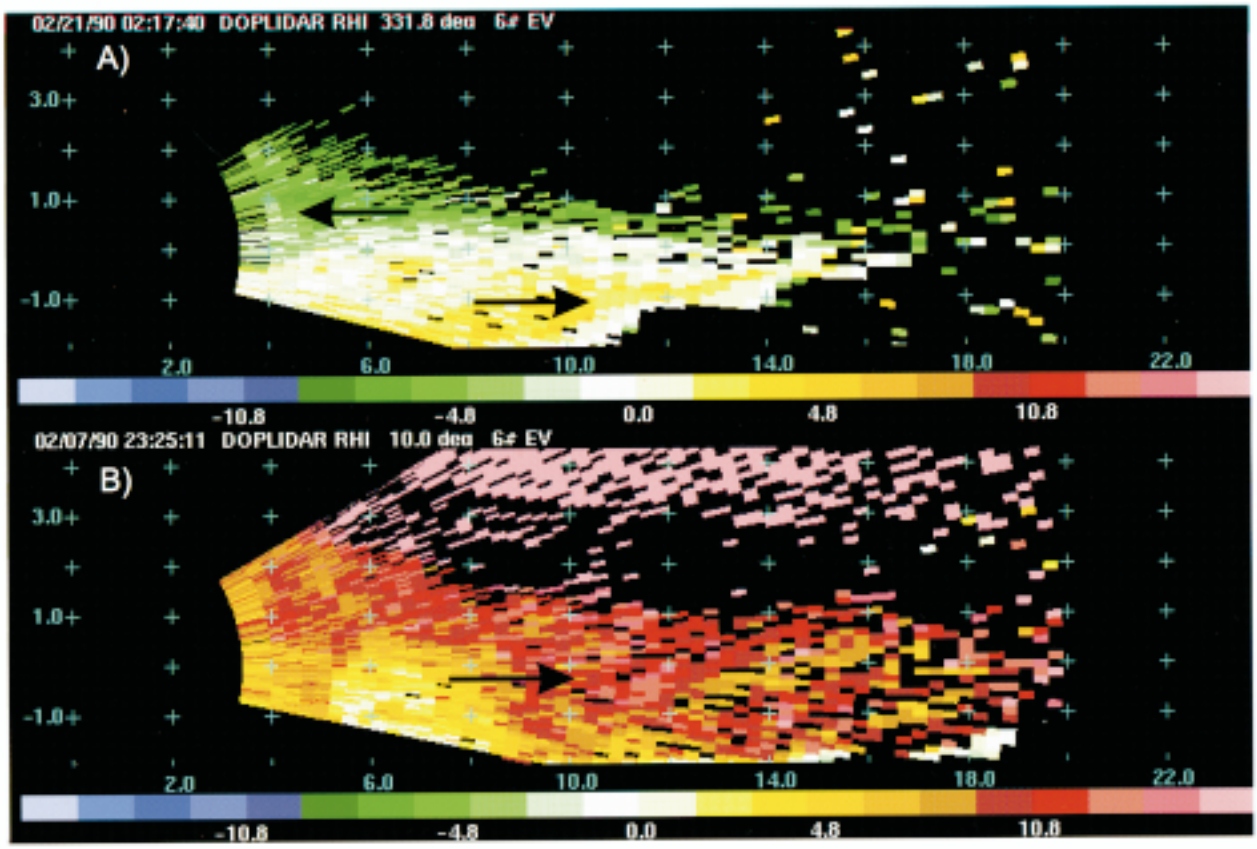

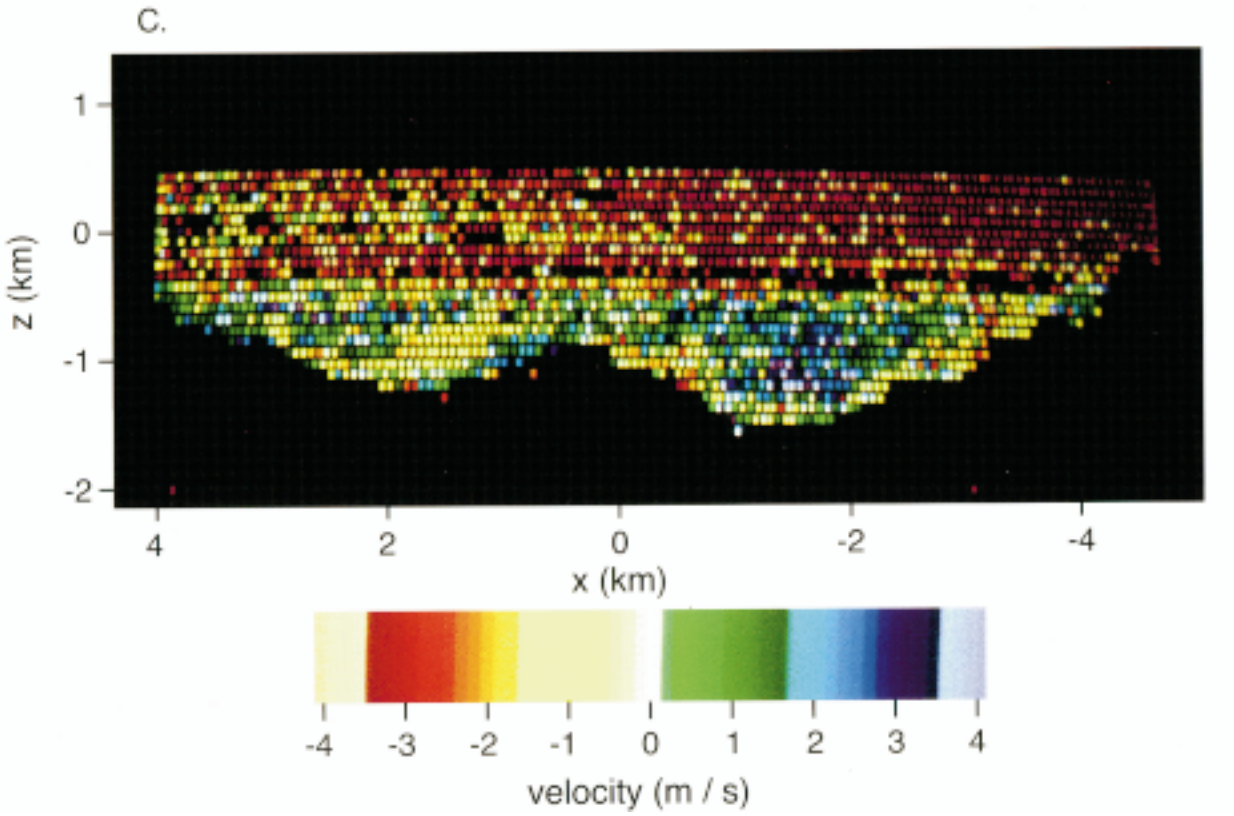

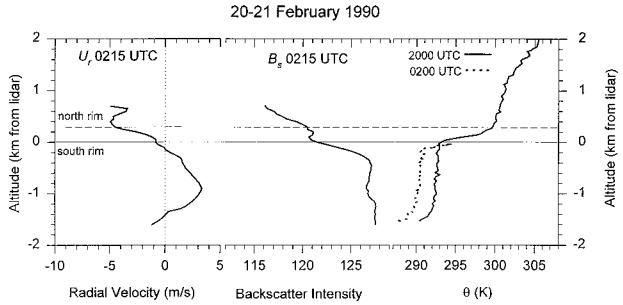

FIG. 6. Vertical profiles from near the canyon bottom to above the south rim showing the radial velocity (u_r, m s^{-1}) and backscatter intensity (B_s in dB), from a Doppler lidar scan on 21 February 1990 at 0215 UTC. Also shown are potential temperature profiles (θ in K), from the Phantom Ranch airsonde at 2000 UTC on 20 February (solid line) and from the Phantom Ranch tethersonde at 0200 UTC on 21 February 1990 (dashed line).

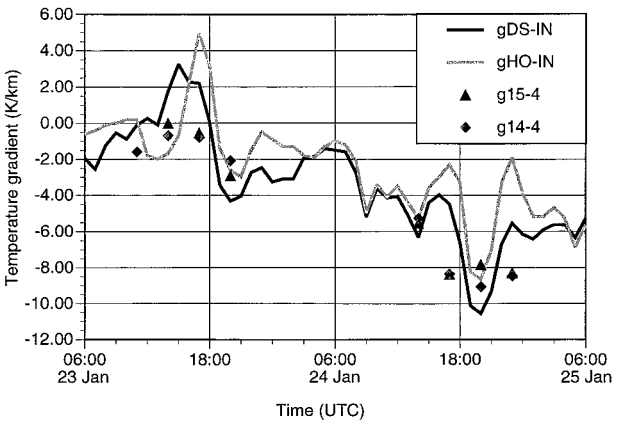

FIG. 8. Hourly values of the stability as measured by surface-station temperature data for 23–25 January 1990 UTC. Also plotted are values from airsonde measurements (▲ and ♦). Temperature gradients: gDS-IN calculated between Desert View and Indian Garden surface stations, gHO-IN between Hopi Point and Indian Garden, g15-4 between the 1500 m and 400 m AGL sounding levels, and g14-4 between 1400 m and 400 m AGL sounding levels.

easterly flow resulting from a traveling cyclone system. Lindsey et al. identified this as a period when emissions arrived at GCNP by ''possible transport through Marble Canyon.'' Banta and Olivier (1991) found that the down-canyon (northerly) flow in the canyon to the north had speeds of ~3 m s^{-1} and concluded that this was sufficient to produce transport of 110 km over a 10-h period, *if* the down-valley flow was continuous in space between the NGS and GCNP, and *if* it persisted in time over the 10–12-h nighttime period. Thus, they concluded, ''in-canyon transport *could* have carried the emittants from the NGS to the Grand Canyon.'' This issue is unresolved, because instrumentation was not sited in the Colorado River gorge to see whether the down-canyon flow was continuous from near the NGS to the Grand Canyon and whether NGS emissions actually made it into the gorge. Because of accessibility and expense considerations, the Doppler lidar provided the only data in the gorge south of Lee's Ferry (near Page) except for Phantom Ranch.

Along with the contour plots, we also used the 3D volume data to produce vertical profiles of u_r, which correspond to mean up- and down-canyon wind speeds through the jet (Fig. 11). The maximum magnitude of northerly flow (negative values) on this profile was 3.1 m s^{-1} at $z = -1.3$ km. Winds decreased with height to zero at -0.6 km and became southerly (positive values) above in the upper portions of the canyon.

To investigate the time-dependent behavior of the jet, we extracted values of u_r at two levels from wind profiles (as in Fig. 11) through the jet. One level, at $z = -1.2$ km, sampled the jet flow in the lower part of the canyon, and the other, at $z = -0.2$ km, sampled the flow in the upper part. These values were obtained for each of the four different types of along-canyon volume scan during this study period. [Banta and Olivier (1991) previously performed a similar analysis using only the full (HR) volume scans.] The time plot of these values (Fig. 12) shows that the flow in the jet at $z = -1.2$ km (solid curve) had a distinctive diurnal variation during the first three days of the period (28 February–2 March),

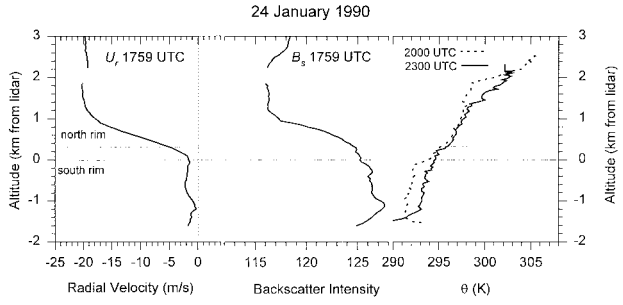

FIG. 7. Vertical profiles of the radial velocity (u_r, m s^{-1}) and backscatter intensity (B_s in dB), as in Fig. 6, except from a Doppler lidar scan on 24 January 1990 at 1759 UTC. Also shown are potential temperature profiles (θ in K), from the Phantom Ranch airsonde at 2000 UTC (dashed line) and at 2300 UTC (solid line).

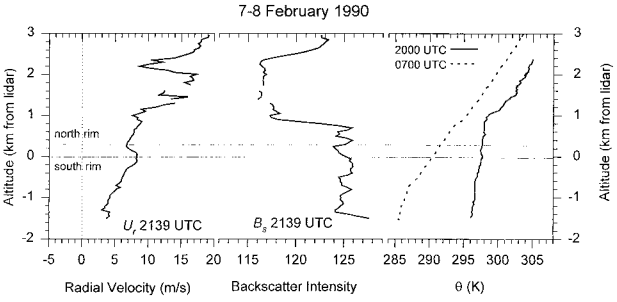

FIG. 9. Vertical profiles of the radial velocity (u_r, m s^{-1}) and backscatter intensity (B_s in dB), as in Fig. 6, except from a Doppler lidar scan on 7 February 1990 at 2139 UTC. Also shown are potential temperature profiles (θ in K), from the Phantom Ranch airsonde at 2000 UTC (solid line) on 7 February, and at 0700 UTC (dashed line) on 8 February.

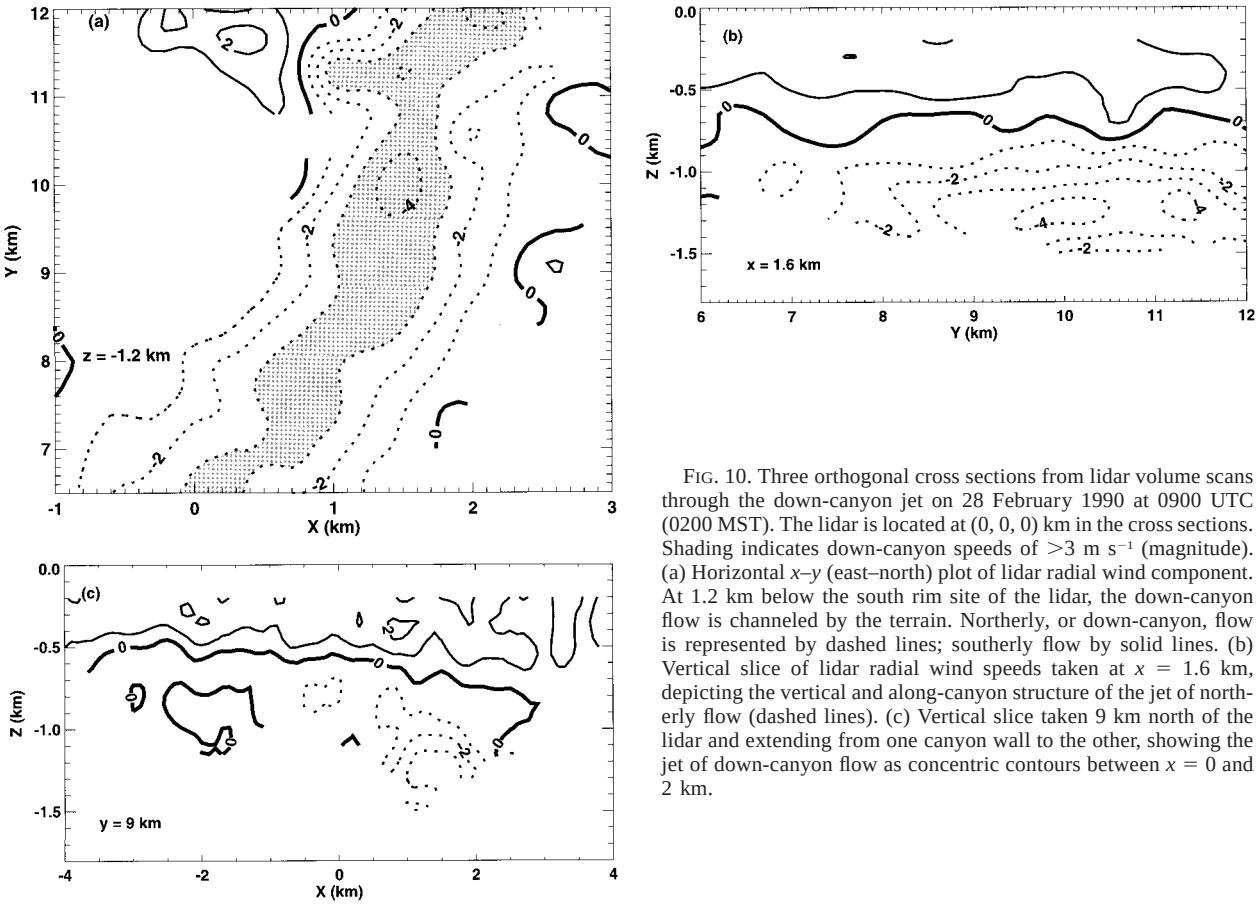

FIG. 10. Three orthogonal cross sections from lidar volume scans through the down-canyon jet on 28 February 1990 at 0900 UTC (0200 MST). The lidar is located at (0, 0, 0) km in the cross sections. Shading indicates down-canyon speeds of >3 m s^{-1} (magnitude). (a) Horizontal x–y (east–north) plot of lidar radial wind component. At 1.2 km below the south rim site of the lidar, the down-canyon flow is channeled by the terrain. Northerly, or down-canyon, flow is represented by dashed lines; southerly flow by solid lines. (b) Vertical slice of lidar radial wind speeds taken at $x = 1.6$ km, depicting the vertical and along-canyon structure of the jet of northerly flow (dashed lines). (c) Vertical slice taken 9 km north of the lidar and extending from one canyon wall to the other, showing the jet of down-canyon flow as concentric contours between $x = 0$ and 2 km.

the velocities becoming increasingly negative through the nighttime hours (shaded).

The flow at sunrise (about 1400 UTC) on these three days was at its peak negative value, indicating strongest down-canyon flow at that time. By around sunset (0000 UTC) on each day the down-canyon flow was at its weakest, having changed sign on one of the days to up-canyon flow. Thus, on these days with very light ambient flow, this analysis shows evidence for thermally forced up-valley/down-valley flow in the bottom of the Grand Canyon.

Also interesting is the response of the flow in the upper half of the canyon. The dashed curve in Fig. 12 shows that the flow at $z = -0.2$ km also varied diurnally during the first three days, but the variation tended to be opposite to the flow in the jet. Banta and Olivier (1991) concluded that the flow in the upper part of the canyon represents a compensating current for the thermally forced flow at the bottom of the canyon, pointing out that this is an example of the behavior one expects from an antivalley/antimountain breeze.

The diurnal rhythm of, and opposite phase relationship between, the flow in the lower and upper portions of the canyon are characteristic of thermally forced up-canyon and down-canyon flows and their compensating return currents. Because of the extreme complexity of the topography in this region, however, other effects could contribute to the cycles of flow in the canyon, especially in the upper region. For example, flows from or into side (tributary) canyons draw air from or spill into the Grand Canyon. Farther north at Marble Canyon the along-canyon component of the diurnal cycle of local up-canyon and down-canyon flows near the surface is opposite to the expected direction, as described in section 2a. These flows are dominated in this area by larger-scale anabatic (upslope) and katabatic (downslope) winds on the Kaibab Plateau and the Marble Platform (Whiteman et al. 1999a,b). Effects such as these probably act or interact with the thermally forced along-canyon flow and return-flow systems farther south in the area of the present study, and thus may be contributing to the behavior shown in Fig. 12.

On 3 March few scans were available because of the snowfall. The winds in the lower canyon on 4 March exhibited the diurnal pattern of increasingly negative wind velocities during the night and more up-canyon (positive) flow the next day.

Later on 4 March and into 5 March, the synoptic flow increased from a southwesterly direction, and this flow was channeled by the canyon. The flow was strong and

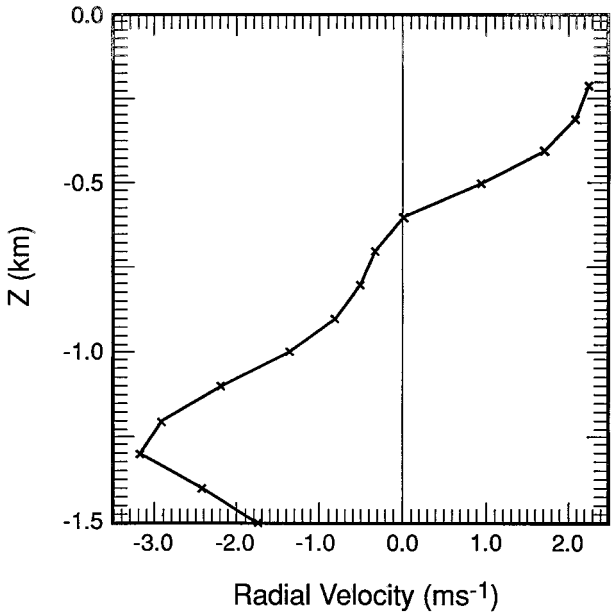

FIG. 11. Vertical profile of mean u_r showing peak speeds of 3.1 m s^{-1} in the jet of down-canyon flow at $z = -1.3$ km, i.e., below the south rim. The wind gradually decreased in speed with height and switched to southerly flow above -0.6 km. The profile, centered at $x = 1.0$ km and $y = 8.6$ km, was from the volume shown in Fig. 10.

turbulent enough to scour the preexisting cooler, cleaner air out of the canyon. As a result, during the last 1½ days of the period, flow in both the upper and lower parts of the canyon was coupled and varied in a similar sense instead of opposite as before. This period was thus representative of the gusty SW flow conditions with strong vertical turbulent mixing, as described in section 3b. Typical of SW flow days, the ambient winds mixed down into the canyon in strongly turbulent flow, and the polluted air, being advected into the region, also mixed down into the canyon. Lindsey et al. (1999) and Richards et al. (1991) identified 5 March as one of the three worst visibility days of the WVS and concluded that pollutants were transported into the region from the urban sources in southern California and Nevada.

2) VERTICAL MIXING

Phantom Ranch θ profiles showed near-neutral stability in the canyon during the day and weak stability (2–3 K km^{-1}) at night (one nighttime profile, 2 March at 0600 UTC, showed a stability as strong as 5 K km^{-1}), during this period. Stabilities above the canyon were near neutral. The gradient between θ in the canyon and that just above also tended to be near neutral, although the sunrise profiles on some days showed a weak ($\sim$1 K) stable jump at the rim.

Time plots of aerosol backscatter at several vertical levels inside and outside the canyon were obtained by Banta and Olivier (1991) from profiles using a procedure similar to that used for u_r in Fig. 12. They noted periods when polluted air was advected into the Grand Canyon region above the rim, for example, 2 and 4 March, and periods when the air was cleaner, for example, 3 March, when it snowed. They found that it took several hours to half a day for air, clean or polluted, to mix downward into the canyon from above the rim, as indicated by changes in the aerosol backscatter.

In contrast to this aerosol-concentration change resulting from canyon airmass replacement, which oc-

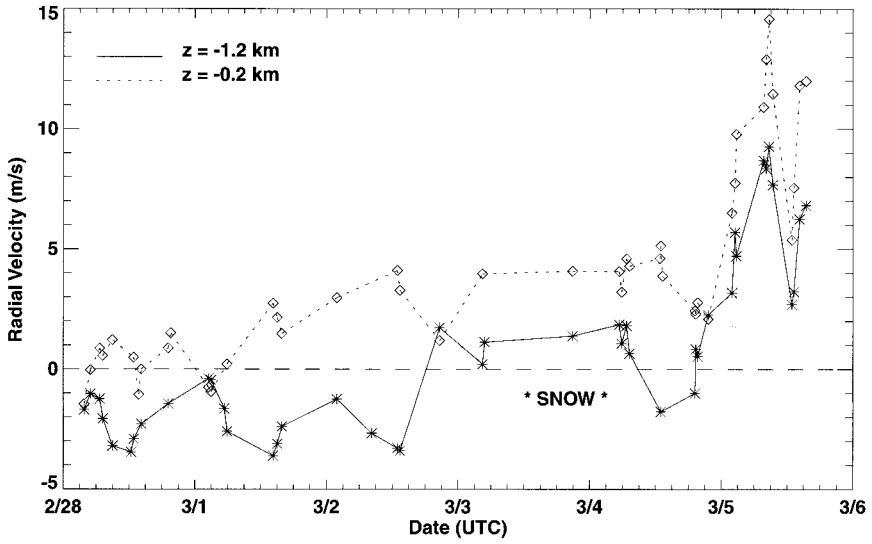

FIG. 12. Radial velocity vs time (UTC) in the lower (solid, *) and upper (dotted, ◊) parts of the canyon. The points were taken from profiles similar to that shown in Fig. 11, and represent horizontal averages between $x = 1.0$ and 1.7 km and $y = 8.0$ and 9.2 km, smoothed in the vertical over 100 m. Shaded areas represent night (local time).

curred over many hours, a change in the lower part of the canyon on 4 March was observed to occur quickly. Because the lidar measured both backscatter and radial-wind data simultaneously, both fields could be analyzed for the same scan sequence. Figures 13–14 show this case, where the joint analysis reveals a case of sudden mixing in the canyon. Figure 13a is a vertical cross section of u_r along the main axis of the canyon, showing that a down-canyon jet persisted in the bottom of the canyon until 1913 UTC (1213 MST) on this day. Figure 13c shows that the jet consisted of relatively low-aerosol-backscatter (''clean'') air, compared with the air in the upper half of the canyon. This indicates a different source for the air in the jet from that for the air just above it. The clean air in the bottom of the canyon may represent the remains of the cooler air mass, which had been in the Grand Canyon region for the previous several days, that the more polluted air was replacing. The difference of 6 dB indicates a difference in backscatter cross section of a factor of 4, which can mean a factor of 4 difference in aerosol concentration, as discussed in section 2b.

Figures 13b,d show conditions 8 min later: both the winds and the aerosol contents were well mixed. This suggests that a weak stable layer had been present during the morning hours, preventing the low-backscatter, down-canyon jet from mixing out, but that the inversion broke because of turbulence-induced mixing at about the time of Figs. 13a,c. After that time, the higher-backscatter air with the southerly momentum component mixed downward rapidly, as the turbulence, produced by surface heating and the gusty SW flow in and above the canyon, coupled the upper and lower parts of the canyon. This mixing and coupling is also illustrated by the midcanyon profiles in Fig. 14. The crossover from negative to positive values of u_r in the lower canyon ($z = -1.2$ km) is evident in Fig. 12.

Figures 13–14 show that the lower canyon can be convectively coupled with the upper canyon under conditions of strong turbulence and surface heating. At these times the timescale for exchange of air between the two regions within the canyon can be very short—a matter of a few minutes—in contrast to the mechanism of canyon airmass replacement, where such exchange could take a half-day or more.

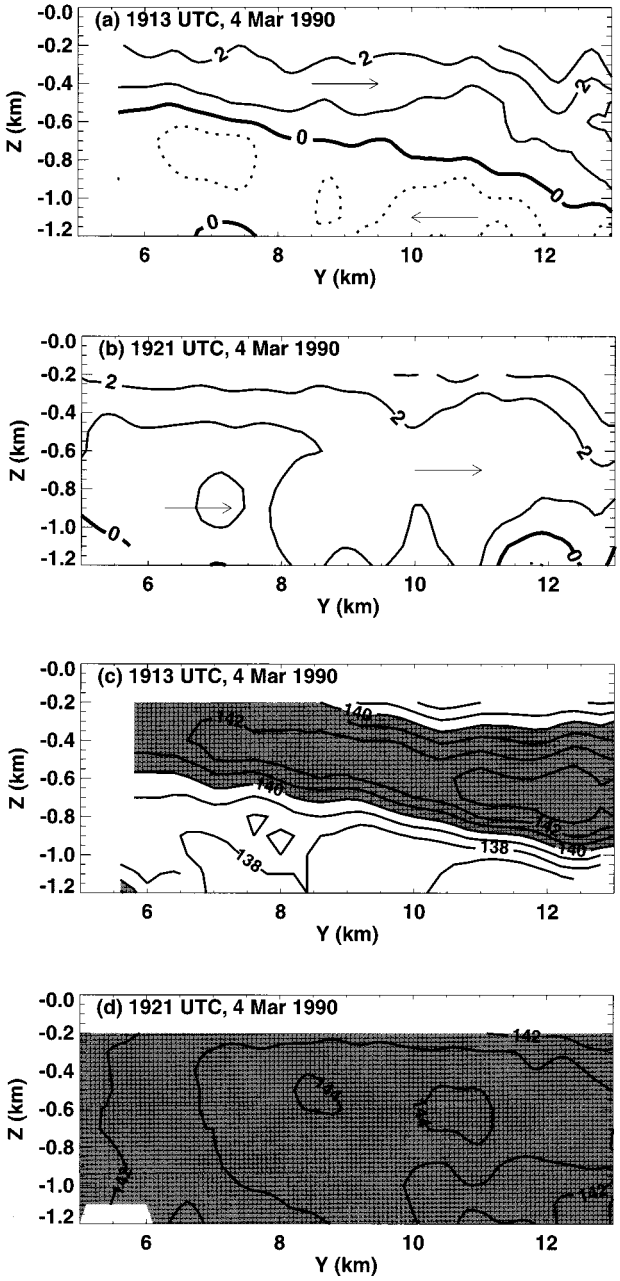

FIG. 13. Upper panels: Along-canyon contours of lidar u_r (m s^{-1}) at (a) 1913 UTC (1213 MST) and (b) 1921 UTC (1221 MST) on 4 March. The lidar was located at (0, 0). Northerly radial velocities >2 m s^{-1} are shaded; the bold zero line separates the northerly flow at the bottom of the canyon from the southerly flow in the upper canyon in (a). Lower panels: contours of aerosol backscatter cross section (dB), at (c) 1913 UTC and (d) 1921 UTC. Intensities >136 dB are shaded, indicating the air with highest backscatter. The highest intensities in the 1913 UTC cross section coincided with southerly winds.

4. Conclusions

Of the many interesting flow regimes in the Grand Canyon revealed by ETL's Doppler lidar, we have focused on three in this study: 1) where the flow in the canyon was in the opposite direction from the cross-canyon flow aloft; 2) where the ambient flow and the flow in the canyon were both southwesterly, generally strong, and turbulent; and 3) where the synoptic flow was weak, and thermally forced up- and down-canyon winds appeared in the canyon. We used the θ and the lidar aerosol-backscatter profile data to infer the effectiveness of vertical mixing in the canyon for each regime. The reversed-flow regime generally occurred with a strong temperature inversion at rim level, and therefore mixing between the air in the canyon and the air just

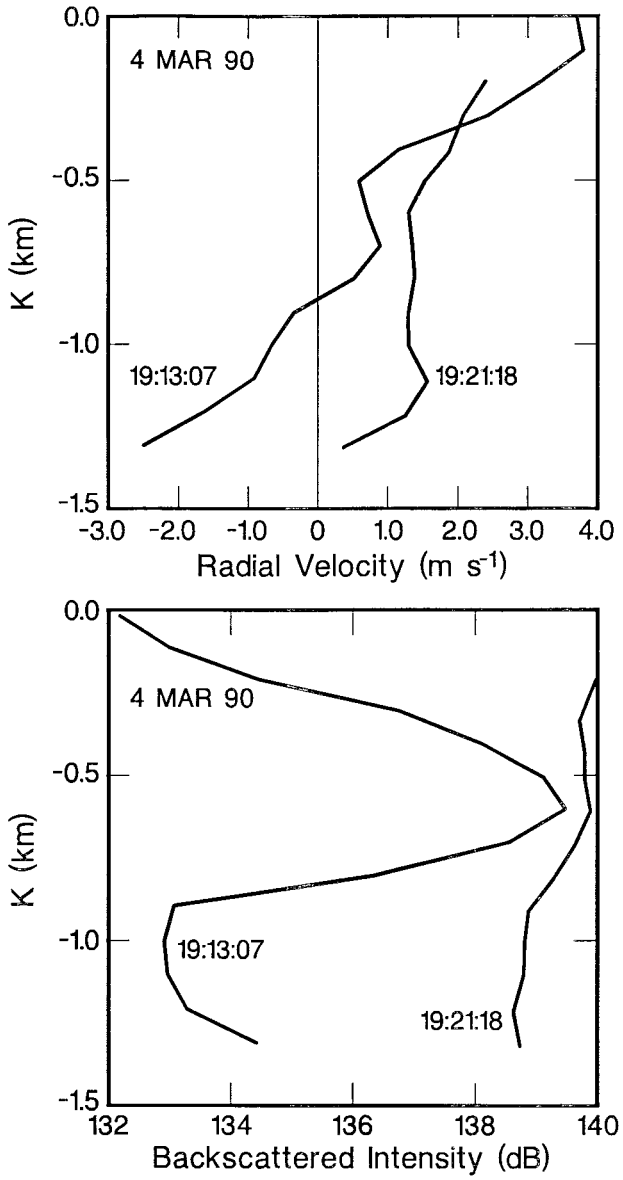

FIG. 14. Profiles of u_r and aerosol backscatter intensity derived from the vertical slices in Fig. 13. Points were calculated by the same process as in Fig. 11.

above was strongly suppressed, although within the canyon the aerosol was well mixed. In the turbulent SW regime, mixing was very efficient both in the canyon and between the canyon and the air above.

In the weak synoptic forcing regime, local, thermally forced flows dominated and vertical exchange within and outside of the canyon was inefficient. The light ambient flow period in this study ended with a transition to polluted, high-aerosol, SW flow, providing an opportunity to assess vertical mixing processes in greater detail. After the high-backscatter air appeared above the canyon, the replacement of the cleaner air in the upper portions of the canyon took several hours to a half-day. This process brought high-aerosol air into the upper canyon, but it did not immediately mix down into the lower canyon. When the two levels finally did mix, it was accomplished by a much faster mixing process within the canyon. Strong turbulent mixing, produced by surface heating and by coupling with the gusty SW winds above, overwhelmed a northerly jet of low-aerosol-backscatter air in the lower canyon in a matter of minutes. Thus, two different vertical mixing processes, one that took many hours and another that took but a few minutes, were observed. It is important, however, to keep these mixing timescales in perspective. These processes were observed when a strong-wind regime eroded the stability in the canyon. In the absence of such a turbulent wind regime, an inversion at the rim top can isolate the canyon from the flow above for several days. Whiteman et al. (1999b) found that strong inversions at the rim are produced by larger-scale warm advection above the canyon. The results of the present study show that if the warm advection is accompanied by strong winds, the inversion may not last very long. The relationship between the effects of wind speed and direction, turbulence, and stability at the rim on the efficiency of vertical mixing into the Grand Canyon is an area that would benefit from further research.

Whiteman et al. (1999b) found no evidence for diurnal flows in tethersonde soundings taken from the Colorado River bank at Phantom Ranch, and Whiteman et al. (1999a) also found that the diurnal along-canyon wind component at certain other locations did not agree with expectation for a thermally forced along-valley wind system. The Doppler lidar, on the other hand, found a distinct diurnal signature to the flow in the Colorado River gorge, a region not sampled by some of the sites such as Buffalo Ranch. The presence of these flows to the north of Desert View and absence at Phantom Ranch indicates that down-valley (and presumably up-valley) flows in a long and serpentine gorge, such as that of the Colorado River, may be discontinuous, with individual segments of the flow being driven by local gradients of the terrain amplification factor (Steinacker 1984; McKee and O'Neal 1989; see Whiteman 1990). If this picture is accurate, then convergence and divergence at the ends of the flow segments would contribute to vertical exchange or transport in the valley (or canyon).

Whiteman et al. (1999b) also showed that cooling and heating in the Grand Canyon tends to occur more uniformly with height than in smaller valleys studied in Colorado, where these processes, especially the cooling, are concentrated at the valley bottom and sidewalls. In this study we also found the aerosol backscatter to be rather uniformly distributed with height, especially in the reversed-flow and SW regimes. These regimes are characterized by eddies or circulations in the canyon that are externally imposed and similar in scale to the dimensions (width or depth) of the canyon. It is likely that these eddies or circulations are responsible for the

vertical transport that produces the uniform profiles of aerosol distribution in the canyon. This implies that these flow structures may also have a key role in distributing daytime heating and nocturnal cooling in the vertical.

Acknowledgments. Support for our involvement in the field effort of the NGS Visibility Study and for part of the analysis presented here was provided by the Salt River Project, Phoenix, Arizona (with special appreciation to program manager Prem Bhardwaja). We thank Matt Savoie for his skillful programming and data-analysis support, John Gaynor and M. J. Post for their critical reviews of this paper, and Christine Sweet for her technical editing of the manuscript. We also appreciate the many helpful discussions with our colleagues Dan Wolfe, Cat Russell, Bill Neff, Dave Whiteman, Rollie Hauser, Lin Lindsey, Joe Sutherland, and Will Richards. Finally we are deeply indebted to the other members of our group, the Atmospheric Lidar Division, for the many long days (and in some cases weeks) spent at the Grand Canyon obtaining this outstanding dataset. The members include M. J. Post, Ron Willis, Janet Intrieri, Kathleen Healy, Mike Hardesty, Wynn Eberhard, Ron Richter, Eric Holloway, Jim Allard, Guy Pearson, and especially Richard Cupp. We appreciate the helpfulness and cooperation of Park Rangers of the National Park Service at Grand Canyon National Park in locating a suitable site for ETL's Doppler lidar.

REFERENCES

Banta, R. M., 1995: Sea breezes shallow and deep on the California coast. *Mon. Wea. Rev.,* **123,** 3614–3622.

——, and L. D. Olivier, 1991: Doppler lidar observations of airflow in the Grand Canyon. *Proc. 84th Annual Meeting, Air & Waste Management Association,* Vol. 2, Vancouver, BC, Canada, AWMA, 1–16.

——, ——, E. T. Holloway, R. A. Kropfli, B. W. Bartram, R. E. Cupp, and M. J. Post, 1992: Smoke column observations from two forest fires using Doppler lidar and Doppler radar. *J. Appl. Meteor.,* **31,** 1328–1349.

——, ——, W. D. Neff, D. H. Levinson, and D. Ruffieux, 1995: Influence of canyon-induced flows on flow and dispersion over adjacent plains. *Theor. Appl. Climatol.,* **52,** 27–42.

——, ——, P. H. Gudiksen, and R. Lange, 1996: Implications of small-scale flow features to modeling dispersion over complex terrain. *J. Appl. Meteor.,* **35,** 330–342.

——, and Coauthors, 1997: Nocturnal cleansing flows in a tributary valley. *Atmos. Environ.,* **31,** 2147–2162.

Bell, R. C., and R. O. R. Y. Thompson, 1980: Valley ventilation by cross winds. *J. Fluid. Mech.,* **96,** 757–767.

Browning, K. A., and R. Wexler, 1968: The determination of kinematic properties of a wind field using Doppler radar. *J. Appl. Meteor.,* **7,** 105–113.

Chan, M., and P. Bhardwaja, 1991: A synopsis of the Navajo Generating Station Visibility Study field project. *Proc. 84th Annual Meeting, Air & Waste Management Association,* Vol. 2, Vancouver, BC, Canada, AWMA, 1–15.

Cunningham, W. J., and A. J. Bedard, 1993: Mountain valley evacuation by upper level flows: A scale model study. *AIAA J.,* **31,** 1569–1573.

Gaynor, J. E., and R. M. Banta, 1991: Relation between cross-canyon circulations and vertical mixing into the Grand Canyon. Preprints, *Seventh Conf. on Applications of Air Pollution Meteorology,* New Orleans, LA, Amer. Meteor. Soc., 384–387.

Hauser, R. K., C. D. Whiteman, and J. L. Sutherland, 1991: Surface meteorological conditions during the Winter 1990 Navajo Generating Station Visibility Impairment Study. *Proc. 84th Annual Meeting, Air & Waste Management Association,* Vol. 2, Vancouver, BC, Canada, AWMA, 1–27.

Levinson, D. H., and R. M. Banta, 1995: Observations of a terrain-forced mesoscale vortex and canyon drainage flows along the Front Range of the Colorado Rockies. *Mon. Wea. Rev.,* **123,** 2029–2050.

Lindsey, C. G., J. Chen, T. S. Dye, L. W. Richards, and D. L. Blumenthal, 1999: Meteorological processes affecting the transport of emissions from the Navajo Generating Station to Grand Canyon National Park. *J. Appl. Meteor.,* **38,** 1031–1048.

McKee, T. B., and R. D. O'Neal, 1989: The role of valley geometry and energy budget in the formation of nocturnal valley winds. *J. Appl. Meteor.,* **28,** 445–456.

McKendry, I. G., D. G. Steyn, R. M. Banta, W. Strapp, K. Anlauf, and J. L. Pottier, 1998: Daytime photochemical pollutant transport over a tributary valley lake in southwestern British Columbia. *J. Appl. Meteor.,* **37,** 393–404.

Mohr, C. G., L. J. Miller, R. L. Vaughn, and H. W. Frank, 1986: Merger of mesoscale data sets into a common Cartesian format for efficient and systematic analysis. *J. Atmos. Oceanic Technol.,* **3,** 143–161.

Neff, W. D., 1990: Remote sensing of atmospheric processes over complex terrain. *Atmospheric Processes over Complex Terrain, Meteor. Monogr.,* No. 45, Amer. Meteor. Soc., 173–228.

Oke, T. R., 1988: Street design and urban canopy layer climate. *Energy Build.,* **11,** 103–113.

Post, M. J., 1978: Experimental measurements of atmospheric aerosol inhomogeneities. *Opt. Lett.,* **2,** 166–168.

——, and W. D. Neff, 1986: Doppler lidar measurements of winds in a narrow mountain valley. *Bull. Amer. Meteor. Soc.,* **67,** 274–281.

——, and R. E. Cupp, 1990: Optimizing a pulsed Doppler lidar. *Appl. Opt.,* **29,** 4145–4158.

Richards, L. W., C. L. Blanchard, and D. L. Blumenthal, Eds., 1991: Navajo Generating Station Visibility Study Final Rep. STI-90200-1124-FR. Prepared for Salt River Project by Sonoma Technology, Inc., Santa Rosa, CA, 408 pp. [Available from Salt River Project, P. O. Box 52025, Phoenix, AZ 85072–2025.]

Rotach, M., 1993a: Turbulence close to a rough urban surface. Part I: Reynolds stress. *Bound.-Layer Meteor.,* **65,** 1–28.

——, 1993b: Turbulence close to a rough urban surface. Part II: Variances and gradients. *Bound.-Layer Meteor.,* **66,** 75–92.

Scorer, R. S., 1978: *Environmental Aerodynamics.* Ellis Horwood, 487 pp.

Sini, J.-F., S. Anquetin, and P. G. Mestayer, 1996: Pollutant dispersion and thermal effects in urban street canyons. *Atmos. Environ.,* **30,** 2659–2677.

Stearns, L. P., 1987: Aspects of local circulation at the Grand Canyon during the fall season. *J. Climate Appl. Meteor.,* **26,** 1392–1400.

Steinacker, R., 1984: Area-height distribution of a valley and its relation to the valley wind. *Contrib. Atmos. Phys.,* **57,** 64–71.

Sutherland, J. L., 1991: Air mass stability associated with winter haziness at Grand Canyon National Park. *Proc. 84th Annual Meeting, Air & Waste Management Association,* Vol. 2, Vancouver, BC, Canada, AWMA, 1–8.

Tang, W., 1976: Theoretical study of cross-valley wind circulation. *Arch. Meteor. Geophys. Bioklimatol.,* **25A,** 1–18.

Whiteman, C. D., 1990: Observations of thermally developed wind systems in mountainous terrain. *Atmospheric Processes in Complex Terrain, Meteor. Monogr.* No. 45, Amer. Meteor. Soc., 5–42.

——, X. Bian, and J. L. Sutherland, 1999a: Wintertime surface wind patterns in the Colorado River Valley. *J. Appl. Meteor.,* **38,** 1118–1130.

——, S. Zhong, and X. Bian, 1999b: Wintertime boundary layer structure in the Grand Canyon. *J. Appl. Meteor.,* **38,** 1084–1102.